Materials Transactions, Vol. 51, No. 4 (2010) pp. 699 to 706

Tensile Deformation and Failure Behavior of Open Cell Nickel and Copper Foams

Shojiro Ochiai[1], Satoshi Nakano[1,*], Yuya Fukazawa[1,*], Mohamed Shehata Aly[1], Hiroshi Okuda[1], Komei Kato[2], Takeshi Isobe[3], Koichi Kita[4] and Keiichi Honma[3]

[1]*Department of Materials Science and Engineering, Kyoto University, Kyoto 606-8501, Japan*
[2]*Mitsubishi Materials Corporation, Saitama 330-8508, Japan*
[3]*Non-ferrous Alloys Research & Technology Laboratory, Mitsubishi Materials Corporation, Kitamoto 364-0023, Japan*
[4]*Central Research Institute, Mitsubishi Materials Corporation, Kitamoto 364-0022, Japan*

Tensile deformation and failure behavior at room temperature of the open cell nickel and copper foams with high porosity (≈96%) fabricated with the slurry foaming process at Mitsubishi Materials Corporation, Japan, was studied. *In-situ* observation of the deformation and failure behavior was conducted with a digital microscope. Stress-strain curves were measured, in which a non-contact extensometer was employed to detect the strain of the samples accurately. Electric resistance was measured to monitor the damage evolution. Finite element stress analysis was conducted to calculate the morphological change of cells with applied strain and the stress distribution in cells. It was revealed that the deformation and failure progressed through the following four stages; stage I characterized by the elastic deformation, stage II by plastic deformation, stage III by the co-occurrence of plastic deformation and cumulative failure of struts and stage IV by the chain reaction of strut failure nearly in a limited cross-section, respectively. Also it was found that the distribution of failure strain of struts in stage III, measured from the serrations in the stress-strain curve, could be described by the Weibull distribution, with which the transition from stage II to III was identified. Also, the result of the statistical analysis suggested that the average failure strain of the struts in the foam is much higher than the strain at ultimate stress of the foam. [doi:10.2320/matertrans.M2009383]

(Received November 19, 2009; Accepted January 19, 2010; Published March 3, 2010)

Keywords: *nickel foam, copper foam, deformation and failure process*

1. Introduction

As the metal foams have the specific features such as light weight, high specific surface area, high potential to absorb impact energy, high air and water permeability and good acoustic insulating properties and so on, they are attractive for industrial application to light weight construction, crash energy absorption, noise control, filtration of solid particles in liquid and gas, heat exchangers, supports for catalysts, water purification, battery electrodes and so on.[1–3] Both in structural and functional applications, mechanical stresses are exerted on metal foams during machining and assembling, and also during service, due to which the mechanical behavior is one of the most important research subjects.

Until now, a wide variety of manufacturing methods, such as gas-injection method,[4,5] directional solidification method,[3,6,7] precursor method,[8–10] slurry foaming method[11] and so on[12–15] has been developed. Among them, the slurry foaming method, in which the metal powders with specific particle size are admixed at room temperature with a foaming agent to form foamy slurry, and the green samples are dried and then sintered under controlled atmosphere at high temperature. This method produces open cell structure with very high porosity fraction (90∼97%).[11] In the present work, the nickel and copper foams manufactured by this method were studied to reveal the deformation and failure process.

2. Experimental and Analytical Procedure

Open cell nickel and copper foam-plates with porosity volume fraction ≈96% and average pore size ≈600 μm, fabricated by the slurry foaming method[11] at Mitsubishi Materials Corporation, were used. The thicknesses of the nickel and copper foam plates were 2.0 and 1.5 mm on average, respectively. The structure of the (a) nickel and (b) copper foams is shown in Fig. 1. The cell structure is composed of struts and nodes as indicated in Fig. 1(a).

Tensile test was carried out at room temperature with a tensile machine (AUTOGRAPH-AG 50kNG, Shimadzu Corp). The width and whole length of tensile samples were 10 and 120 mm, respectively. Both ends of the tensile samples are glued to aluminum tabs with an epoxy-glue, as shown in Fig. 2(a). The test was conducted at a constant crosshead speed of 8.3×10^{-6} m·s^{-1}.

Strain of samples was measured with a non-contact extensometer due to the following reasons. The porosity volume fraction of the present samples was high (≈96%) and the metals (pure nickel and copper) were soft. The strain gages were not suitable for measurement of the sample strain due to the constraint, even small, of the deformation of cells at the gage-adhered parts and due to the narrow covered area which gives, more or less, only local information. The usual extensometer was also not suitable due to its weight that can cause bending of samples. In the measurement of the strain of the sample itself with a non-contact extensometer, two markers made of paper were pasted on the samples, whose spacing was 50 mm, as shown in Fig. 2(a). The displacement of the markers was recorded with a laser CCD camera (DVW-200 Shimadzu), as shown in Fig. 2(b).

To monitor the progress of failure, the change of the electric resistance with strain was measured with a usual four probe method. The deformation and failure behavior was observed *in-situ* with a digital microscope (KEYENCE VHX-500SP1639).

The changes of the morphology of the cell and stress distribution in the deformed cell were analyzed with a finite

*Graduate Student, Kyoto University

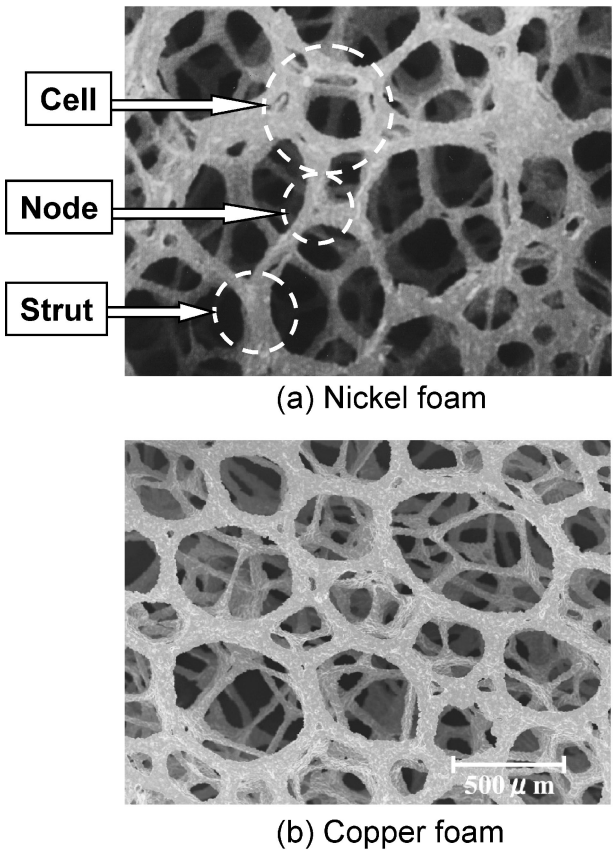

Fig. 1 Structure of (a) the nickel- and (b) copper-foams fabricated by slurry foaming process at Mitsubishi Materials Corporation.

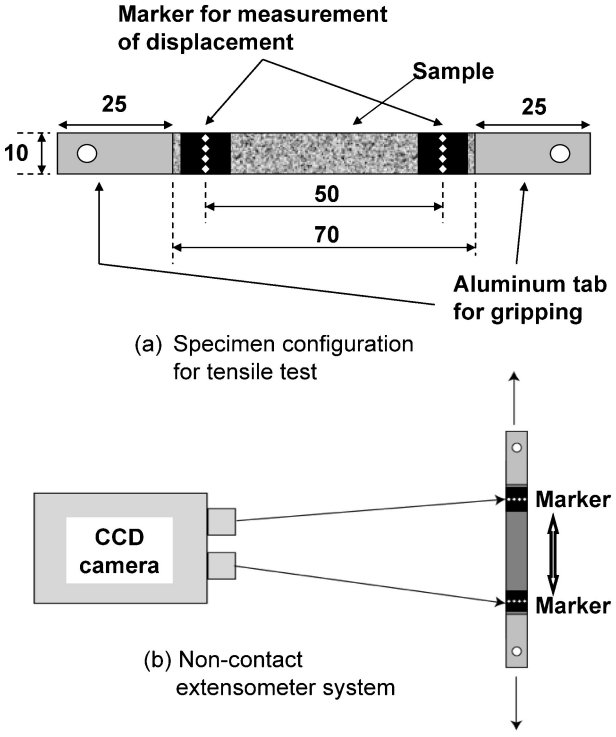

Fig. 2 Schematic representation of (a) specimen configuration for tensile test and (b) non-contact extensometer system for measurement of displacement of specimen.

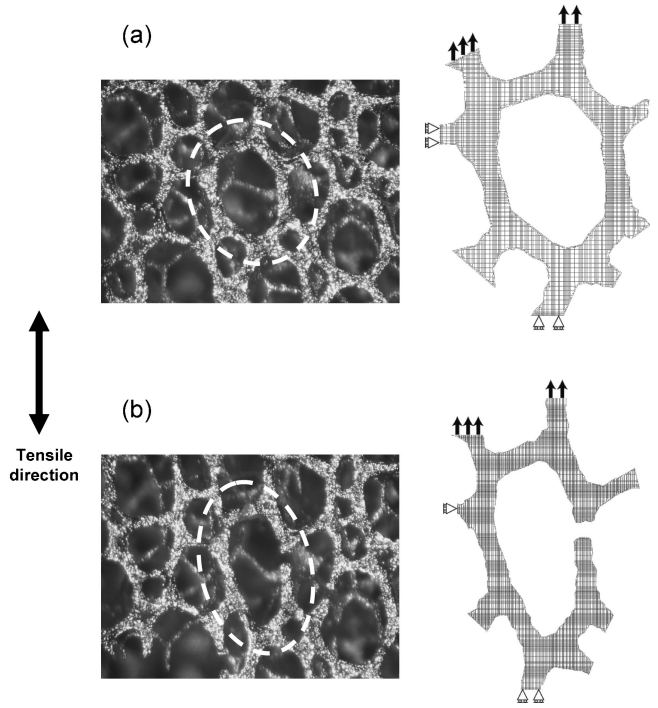

Fig. 3 Modeling and boundary conditions for FEM analysis of the deformation and fracture behavior of the cell. (a) and (b) show (left side) the observed morphologies and (right side) FEM models taken from the cells indicated by the broken circles, referring to the situation before and after a failure of the strut, respectively.

element analysis. Figure 3(a) and (b) shows the observed shapes of the non-damaged and damaged cells in the copper foam, respectively. The observed morphologies were modeled as shown in the right sides to calculate the stress state. Hereafter the model in (a) is called as the cell model without a failed strut and that in (b) as the cell model with a failed strut. In this modeling, two dimensional model was used in accordance with the two dimensional observation. Though the present modeling is rough, the experimentally observed morphological change of cells could be reproduced and also important indications concerning the stress-state could be read, as will be shown later in 3.3. As the externally applied strain is transferred to the cell mainly by the struts parallel to the tensile axis, the boundary conditions were given as shown in the models in Fig. 3. The stress analysis was carried out using a commercial finite element code MARC/Mentat™ under the plane stress condition. The yielding condition for the copper was given by the von Mises criterion.

As the mechanical properties of the copper in the present foam were unknown, the following values reported for full annealed polycrystalline copper[16] were used: Young's modulus $E_{cu} = 110\,\text{GPa}$, Poisson's ratio $= 0.343$, tensile strength $(\sigma_{UTS}) = 210\,\text{MPa}$, yield stress $(\sigma_Y) = 33.3\,\text{MPa}$ and nominal strain at ultimate stress $(e_{UTS}) = 60\%$. From these reported values, the true stress (σ_t)–true strain (ε) curve of copper was expressed with the Ludwik's equation given by

$$\sigma_t = \sigma_y + K(\varepsilon - \varepsilon_y)^n \tag{1}$$

where ε_y is the yield strain, and K and n are the constants. Using the well known expressions in solid mechanics, we have $\varepsilon_y = \sigma_Y/E_{Cu}$ (Hooke's law), $\varepsilon = \ln(1+e)$ (relation

between the true (ε) and nominal (e) strains), $\sigma_{UTS} = \{\sigma_y + K(\varepsilon_{UTS} - \varepsilon_y)^n\}\exp(-\varepsilon_{UTS})$ (relation of the nominal tensile strength (σ_{UTS}) to the true strain (ε_{UTS}) at ultimate stress), and $[d\{\sigma_t \exp(-\varepsilon)\}/d\varepsilon](d\varepsilon/de) = 0$ at $e = e_{UTS}$ (necking condition). Substituting the reported mechanical property values mentioned above into these relations, we had $\varepsilon_y = 3.03 \times 10^{-4}$ ($\sigma_y = 33.3$ MPa), $n = 0.467$ and $K = 432$ MPa for eq. (1).

3. Results and Discussion

3.1 Stress-strain curve and change of electric resistance with strain

The nominal stress-nominal strain and electric resistance-nominal strain curves, measured at the same time, of the nickel- and copper-foams are presented in Fig. 4(a) and (b), respectively. The stress-strain curve in the rectangle in Fig. 4(b) is presented at high magnification in Fig. 4(c). The following features are found in Fig. 4.

(1) In the initial stage, the foams deform elastically. The strain range of this stage was very narrow, around 0.01% for both foams.

(2) After yielding, the most parts of foams deform plastically, as shown later in 3.3. With further increasing applied strain, serrations appear in the stress-strain curve as shown in (c), in which the serrated parts are shown with circles. Such serrations are attributed to the failure mainly of the struts, as ascertained by the observation (details will be presented later in 3.2). In each serration, the stress drops due to the strut failure-induced loss of stress carrying capacity of the foams and then increases due to the strain hardening of the constituting metals. In the strain range up to the strain at ultimate stress (5.2 and 6.2% for nickel and copper foams, respectively), the stress increases after each serration. This means that the failure of struts occurs independently to each other and is cumulated in the sample up to the strain at ultimate stress. In other words, even when the struts are failed, they do not cause successive failure of the neighboring struts. Such a failure mode is named as cumulative mode. On the other hand, beyond the strain at ultimate stress, the stress of the foams decreases with increasing strain, suggesting that the failure of struts occurs in the manner to reduce the stress carrying capacity of the foams. As will be shown in 3.2, the failure of the struts occurs successively in a limited cross-section beyond the strain at ultimate stress (successive failure mode). Namely, the failure mode of the struts turns at the strain at ultimate stress from cumulative to successive one.

(3) The electric resistance increases gradually up to the strain at ultimate stress. On the other hand, beyond the strain at ultimate stress, the resistance increases significantly, reflecting the successive failure of struts in a limited cross-section. This means that, when the failure of the struts occurs in a limited cross-section, the current path decreases significantly. The gradual increase in resistance below the strain at ultimate stress is attributed to the failure of the struts and also to the increase in amount of dislocations. The individual effect could not be estimated separately in the present work. However, judging from the significant increase in resistance beyond the strain at ultimate stress, stemming from the failure of the struts in a limited cross-section, it is speculated that the gradual increase in resistance below the strain at ultimate stress stems mainly from the spatially distributed failure of the struts in the specimen volume.

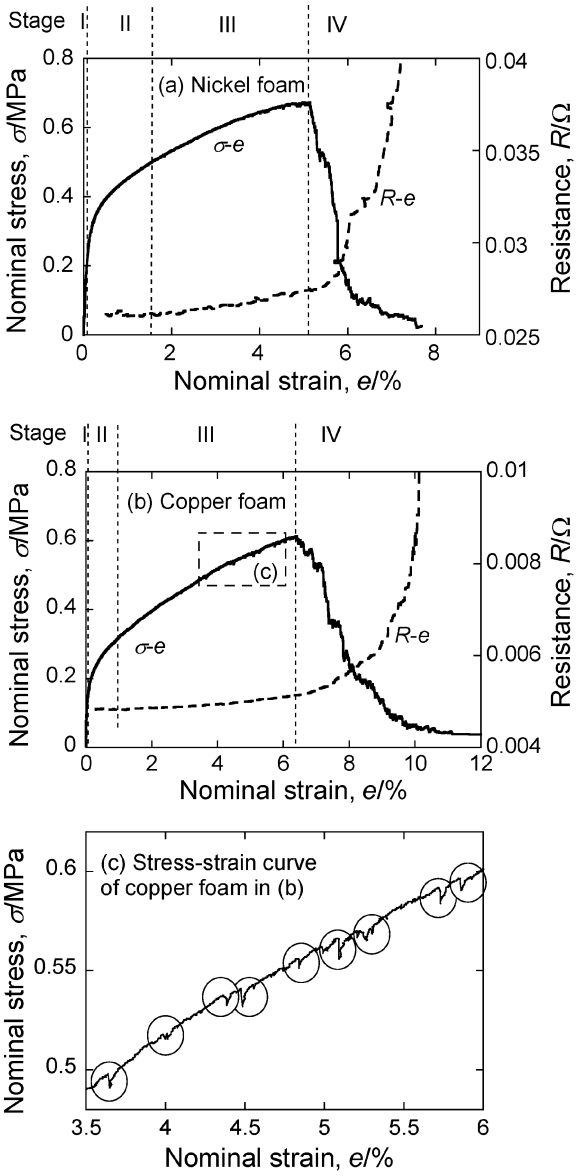

Fig. 4 Nominal stress-nominal strain and electric resistance-nominal strain curves of (a) the nickel- and (b) copper-foams. The stress-strain curve in the rectangle in (b) is presented at high magnification in (c).

(4) The features mentioned above suggest that the deformation and failure progresses through the following four stages; stage I characterized by the elastic deformation, stage II by plastic deformation without failure of struts, stage III by the co-occurrence of plastic deformation and cell failure and stage IV by the successive failure of struts nearly in a limited cross-section, as marked in Fig. 4(a) and (b) for nickel and copper foams, respectively.

Details of the *in-situ* observation results on the failure behavior in the late stage III and stage IV will be presented in 3.2. The change of the shape of cells with increasing applied strain and the stress distribution calculated with a finite element analysis for the model cells in Fig. 3 will be presented in 3.3. An attempt to estimate the strain at transition from stage II to III, based on the statistical

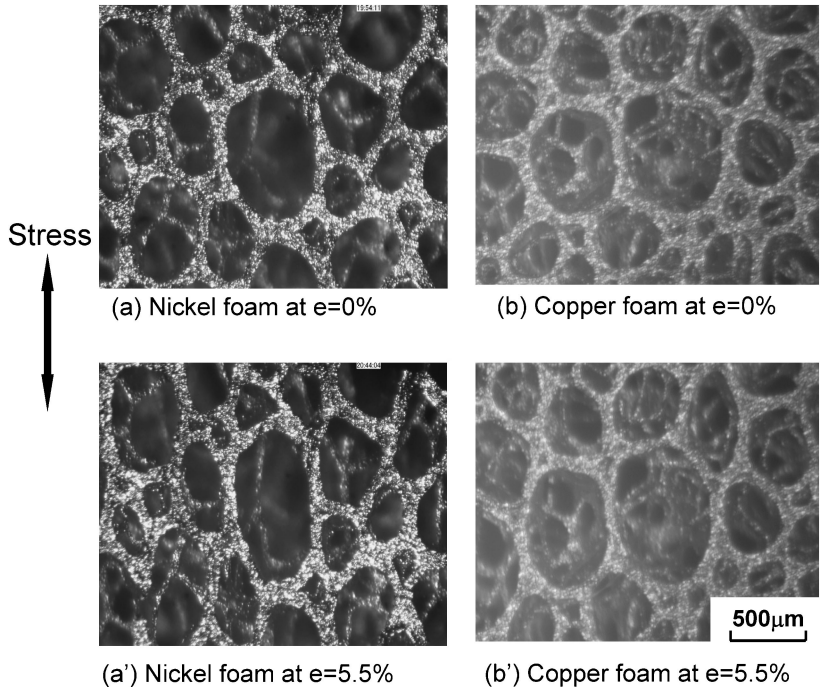

Fig. 5 Change of the shape of the cells with increasing applied nominal strain.

analysis, will be presented in 3.4. Also the condition for the transition of stage III to IV to arise will be discussed in 3.4.

3.2 Observed deformation and failure behavior

Figure 5 shows the morphological change of the foam with increasing applied strain. The shape of the cells is complex, due to which complex stress state is realized, as has been observed by X-ray tomography for other type aluminum foams.[17,18] From the phenomenological viewpoint, the cells are evidently elongated and the struts are straight forwarded along the tensile direction. As shown in Fig. 4, the strain range of elastic deformation (stage I up to around 0.01% strain in both nickel and copper foams) is very narrow. The morphological change is eternal once applied strain exceeds around 0.01%.

The ductile nature of the struts was evidenced by the failure morphology. Both the nickel and copper foams failed similarly in a ductile manner. Figure 6 shows (a) the overall failure surface and (b), (c) failure morphology of the struts in the nickel foam. As shown in (a), the overall failure occurred nearly in a limited cross-section where the difference in height of the failed struts was within one cell size. The reason for this will be discussed in detail later in this sub-section. The struts failed in a ductile manner, accompanied by (b) the cup and cone type and (c) shear lip type morphology. The struts in the present foam are composed of a small number of grains in a cross-section. It is deduced that the crystallographic relation between the grain and tensile direction in (b) is different from that in (c), causing the different failure morphology. In (b), plural slip systems are found and the slip bands are wavy. In this case, possibly due to the intersection of dislocations, voids are formed, resulting in cup and cone type ductile failure. On the other hand, in (c), only one slip system is found and the slip bands are straight. In this case, a shear lip failure occurs.

Figure 7 shows the *in-situ* observation result of the failure process of the nickel foam in stage IV where the struts are failed successively in a limited cross-section. (a) to (e) were observed at the applied strains $e = 5.0$, 5.3, 5.6, 6.0 and 6.6%, respectively. The transition of the failure mode of struts from cumulative to successive occurred at $e = 5.2\%$. In this specimen, the strut having a portion with a very narrow cross-section, indicated by 1 in (a), is failed as shown in (b). Once the strut 1 is failed, the failed-ends in the strut 1 open and the strut 2 originally nearly perpendicular to the tensile direction (b) is elongated toward the direction parallel to the tensile stress (c). As a result, the strut 3 in (c) is stressed more and is failed (d). In this way, the failure of one strut (1 in this specimen) causes the failure of the neighboring strut 3. After the failure of the strut 3, the failed-ends open, which gives high stress to the strut 4. As a result, the strut 4 is failed. Due to such a chain reaction, the neighboring struts are failed successively one after another nearly in a limited cross-section within one cell size in the stress direction. The reason for this is accounted for as follows.

As the cross-sectional area of surviving struts varies along the sample length direction and the stress concentration of the surviving struts enhanced by the preceding failure of the neighboring struts also varies along the length direction, the failure position of each strut is different, namely failure of the foam progresses in a zigzag manner, but as the latter (stress concentration) is enhanced essentially in the struts between upper and lower nodes, the difference in height among the failed struts is within one cell size. Thus, the successive failure of struts in stage IV occurs nearly in a limited cross-section. The failure of the copper foam in stage IV occurs in a same manner to that of the nickel foam (failure of one strut causes the neighboring struts one after another nearly in a limited cross-section.).

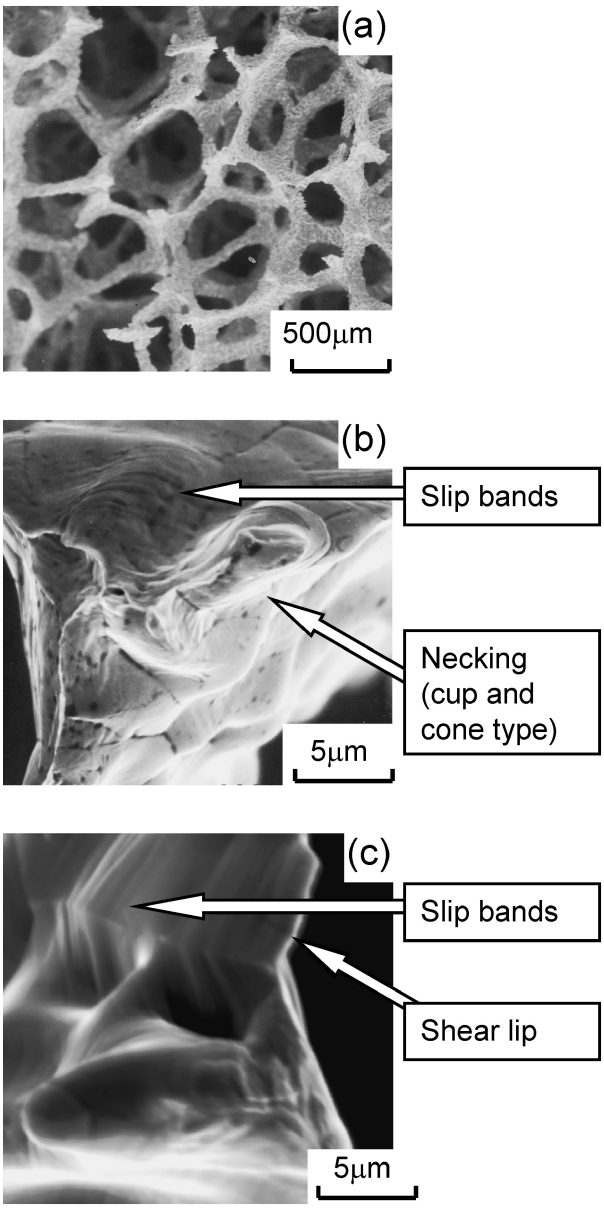

Fig. 6 Failure surface of (a) the nickel foam and (b), (c) struts.

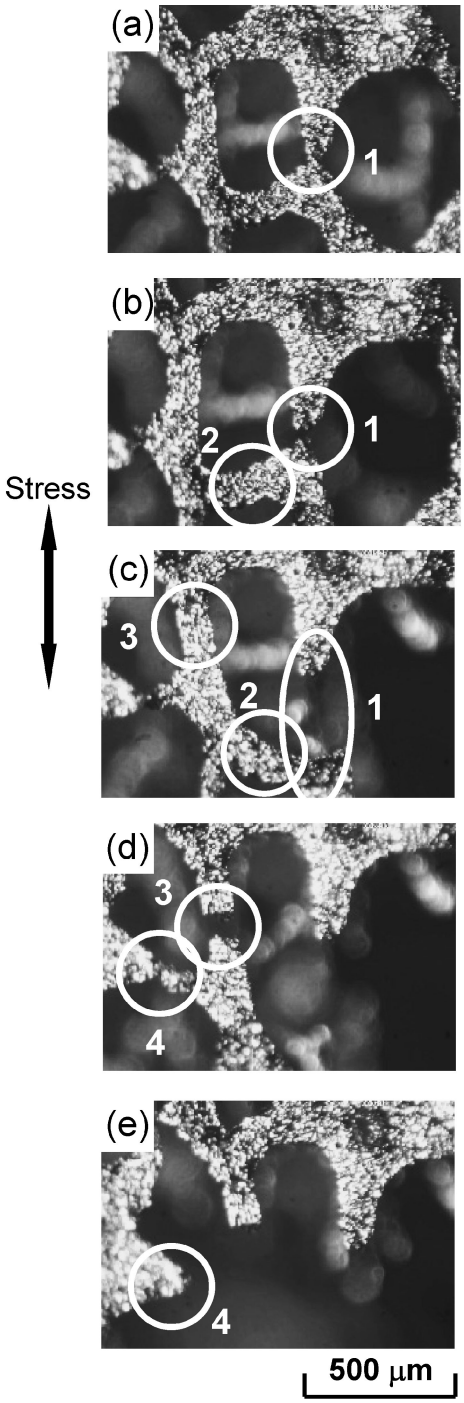

Fig. 7 Observed failure process of the nickel foam in stage IV where the struts are failed successively. e (nominal strain) = (a) 5.0, (b) 5.3, (c) 5.6, (d) 6.0 and (e) 6.6%.

In this way, the morphology change of cells and failure of struts take place in the deformation and failure process of ductile metal foams. The deformation and failure process both of the nickel and copper foams observed in the present work is summarized, as schematically shown in Fig. 8.

3.3 Change of the morphology and stress distribution with increasing applied strain in the cell with and without a failed strut, analyzed with the finite element method

The results analyzed with the finite element analysis using the models of the cell without and with a failed strut shown in Fig. 3(a) and (b) are presented in Figs. 9 and 10, respectively. In these figures, the true stress in the tensile direction is used representatively instead of the equivalent stress, since the tensile and compressive stresses co-exist, which cannot be distinguished if we use the equivalent stress. Initial shape of the cell is also indicated with black lines for comparison. The following features are read from Figs. 9 and 10.

(1) Both cells without and with a failed strut are elongated more in the tensile direction with increasing applied strain. These results are in good accordance with the observation results in Figs. 5 and 7.

(2) In the cell without a failed strut (Fig. 9), tensile stress is exerted in the inner side parts and compressive one in the outer side parts in both struts, as shown in (A) and (B) indicated with blue broken lines in (a). This means that bending stress acts in both struts during elongation of the cell in the tensile direction, stemming from the curved shape of the struts in the original state. With further increasing applied

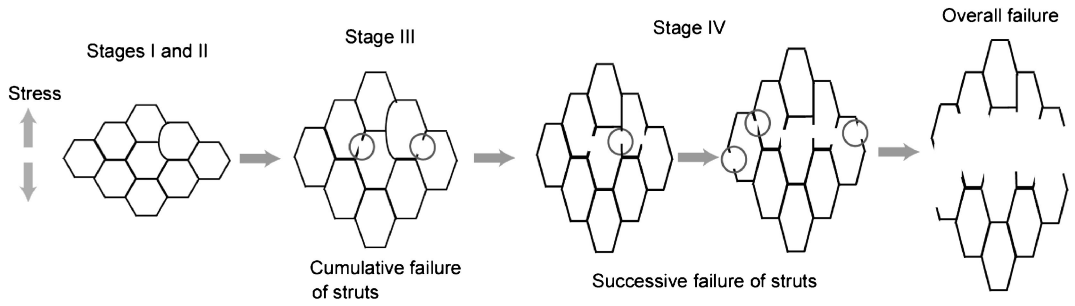

Fig. 8 Schematic representation of the deformation and failure process of the foam, accompanied by the change of morphology and failure of struts. In stages I and II, no struts fail. In stage III, the failure of struts occurs in a cumulative manner, where the failure occurs independently to each other and the failed struts do not cause the failure of neighboring struts. In stage IV at increased applied strain, the failure of struts occur successively nearly in a limited cross-section due to the enhanced stress (strain) on the neighboring struts by the opening of the failed ends of the pre-failed neighboring struts.

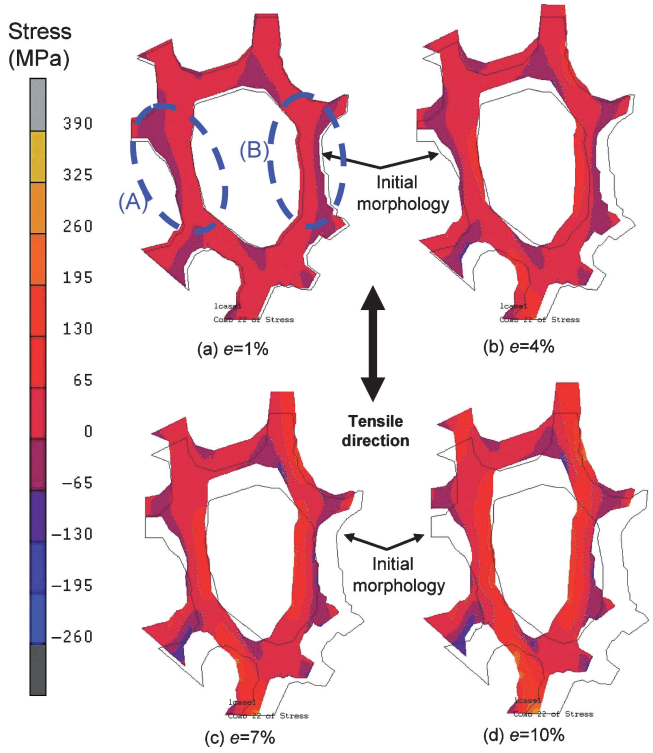

Fig. 9 Calculated change of the morphology and true stress distribution with increasing applied nominal strain in the cell without failed strut.

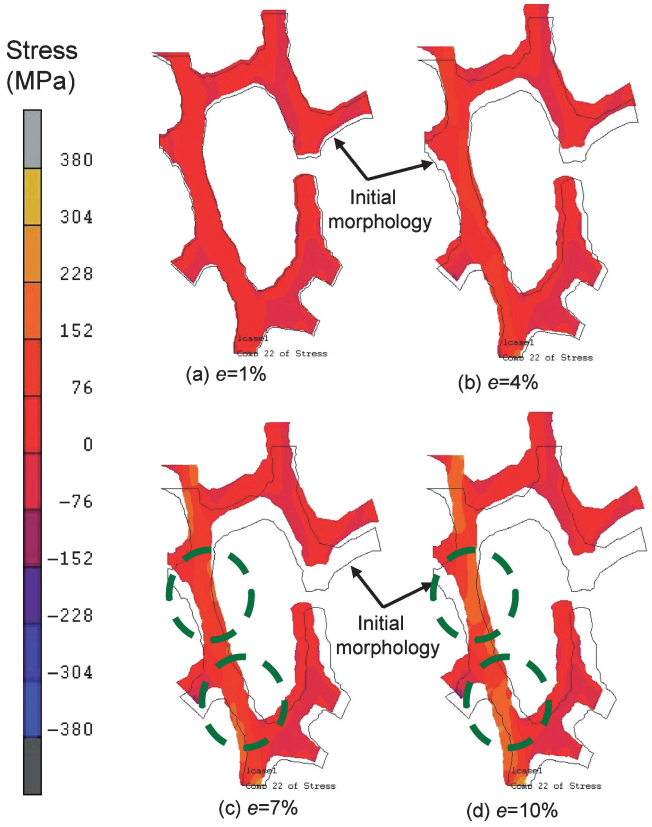

Fig. 10 Calculated change of the morphology and true stress distribution with increasing applied nominal strain in the cell with a failed strut.

strain, the struts elongate along the tensile direction and the compressive stress tends to be diminished.

(3) In the cell with a failed strut (Fig. 10), the opening of the failure ends in the strut increases with increasing applied strain. This phenomenon is in good accordance with the observation result in Fig. 7. It is noted that such an opening enhances the tensile stress of the surviving (non-failed) strut as shown in the green circles in Fig. 10(c) and (d). This result accounts well for the successive failure of struts in stage IV observed in Fig. 7.

3.4 Statistical analysis of failure strain of struts

It has been shown in 3.1 and 3.2 that the failure of the struts occurs cumulatively and successively below and beyond the strain at ultimate stress, respectively. Also it has been shown in 3.3, when a strut fails, the failure ends open, raising the stress concentration at the neighboring struts with increasing applied strain. As shown in these results, the failure of struts plays a dominant role in the determination of failure process and mechanical properties of foams. However, the statistical feature of failure of struts has not been studied in detail until now. In this sub-section, the failure strain of struts in the foam is analyzed statistically. Then, the result is used to determine the initiation of the strut failure, namely the transition strain from stage II to stage III (Figs. 4(a) and (b)) and also to account for the transition from stage III to IV.

As has been shown in Fig. 4(c), the cumulative failure of the struts in stage III is reflected with the serrations in the stress-strain curve. Thus the failure strain e_f of the strut in the foam can be read from the serration. The e_f value in this work

is not the usual failure strain for straight samples. It is dependent on the geometrical relation of the strut to the applied tensile stress direction. For instance, when the strut is just parallel to the tensile axis, the externally applied stress is transferred efficiently and it can be failed at its failure strain. On the other hand, when the strut is largely inclined to the tensile axis, the applied strain is consumed until the stress is transferred efficiently, as in the case of loose strands. Namely the strut needs high strain to be stretched tightly. In the present work, such a geometry-affected failure strain e_f is estimated from the serration.

In the present samples, the stress-strain curves were measured for the test pieces shown in Fig. 2(a). The serrations in the stress-strain curve (Fig. 4(c)) arose from the volume of 10 (width) × 50 (length) × 2.0 (thickness) mm^3 for the nickel foam and from the volume of 10 × 50 × 1.5 mm^3 for the copper foam. The average pore size was 600 μm for both foams. Thus, as a first approximation, total number n of struts in the gage portion, for which the stress-strain curve was measured, was taken to be $n = 4648$ and 3486 for nickel and copper foams, respectively. The cumulative probability F_i of e_f of the i^{th}-failed strut was estimated by the median rank method, expressed by

$$F_i = (i - 0.3)/(n + 0.4) \tag{2}$$

For description of distribution of the e_f values, three parameter Weibull distribution function,[19] which has been used widely for description of strength distribution of materials, was used as a first approximation in this work. According to this function, the cumulative probability F of e_f is expressed by

$$F = 1 - \exp[-\{(e_f - e_{f,min})/e_0\}^m] \tag{3}$$

where e_0 and m are the scale and shape parameters, respectively, and $e_{f,min}$ is the lower bound of e_f. The parameter values of e_0, m and $e_{f,min}$ were estimated as follows.

Equation (3) is re-written in the form,

$$\ln\ln(1 - F)^{-1} = m\ln(e_f - e_{f,min}) - m\ln(e_0). \tag{4}$$

First, various values were assumed for $e_{f,min}$ and the linearity between $\ln\ln(1 - F)^{-1}$ and $\ln(e_f - e_{f,min})$ was examined for each $e_{f,min}$-value. The $e_{f,min}$-value that gave the highest linearity was estimated as the $e_{f,min}$. We had $e_{f,min} = 1.7\%$ for nickel foam and 0.86% for copper foam. For these values, very high linearity is found in the relation of $\ln\ln(1 - F)^{-1}$ to $\ln(e_f - e_{f,min})$, as shown in Fig. 11. The m and e_0 were estimated from the slope and extrapolation of the relation of $\ln\ln(1 - F)^{-1}$ to $\ln(e_f - e_{f,min})$, as indicated in Fig. 11.

As shown above, the values of $e_{f,min}$, m and e_0 were obtained for the assumed number of struts ($n = 4648$ (nickel) and $n = 3486$ (copper) which were calculated using the average cell size). The calculated n corresponds to the minimum case for n among the possible cases since each cell has plural struts. The actual n value is larger. The influence of the n value on the Weibull plot was examined as follows.

Figure 12 shows the Weibull plot in the nickel foam for $n = 4648$, 13944 (three times of 4648) and 46480 (ten times), obtained by the procedure stated above. The $e_{f,min}$ and m values were not affected by n. On the other hand, e_0 value was dependent on n: the larger the n, the larger became the e_0. This result indicates that the obtained value $e_{f,min} = 0.017$

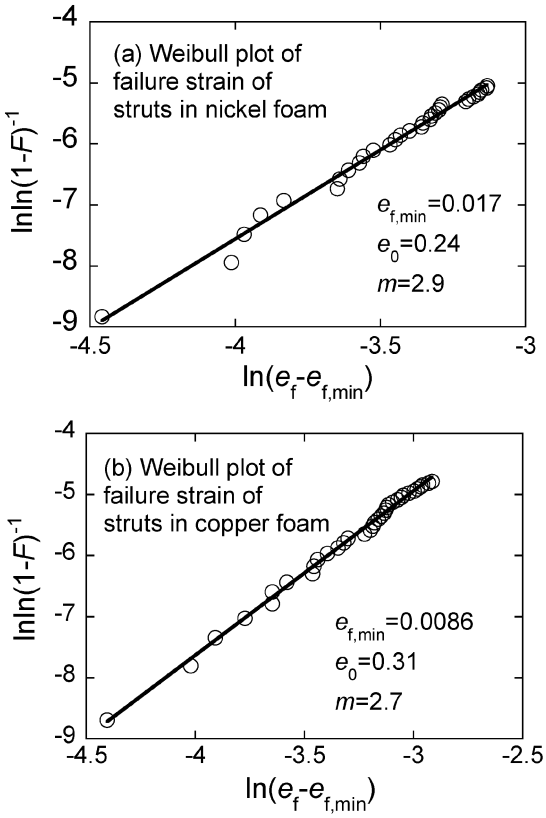

Fig. 11 Weibull plot of the failure nominal strain e_f of the struts in (a) the nickel- and (b) copper-foams and the obtained values of $e_{f,min}$, e_0 and m by regression analysis, where F was calculated for $n = 4648$ (nickel) and $n = 3486$ (copper) based on the average cell size.

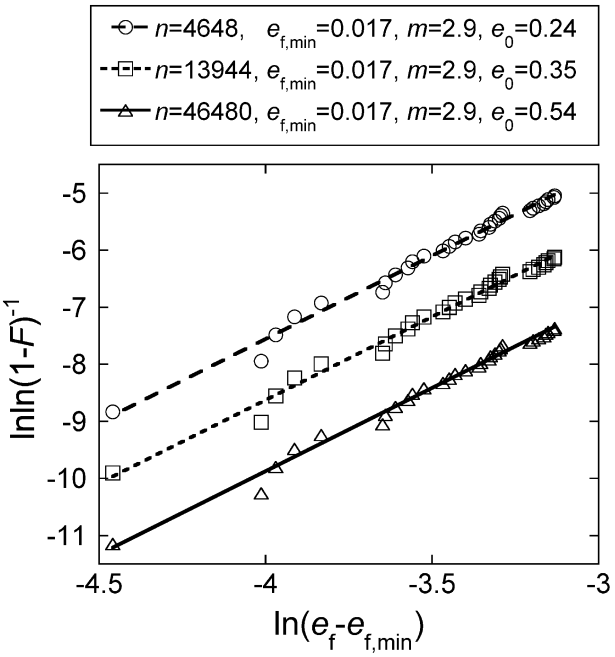

Fig. 12 Weibull plot of the failure nominal strain e_f of the struts in the nickel foam and the obtained values of $e_{f,min}$, e_0 and m by regression analysis, where F was calculated for $n = 4648$, 13944 and 46480.

and $m = 2.9$ are reliable even when the actual n value is unknown, while e_0 value is dependent on n value and it shall be determined for an actual n value.

The reason for this is accounted for as follows. In stage III, the struts with low failure strains are failed cumulatively. In this stage, the number of failed struts is small in comparison with the total number of struts. Thus, eq. (3) is reduced to

$$F = \{(e_f - e_{f,min})/e_0\}^m \quad (5)$$

Also, as F is low, the term $\ln\ln(1-F)^{-1}$ in eq. (4) is reduced to $\ln(F)$. The reduced form of eq. (4) is just same as eq. (5). As the measured e_f values are common for any n value (and for F since F is given by eq. (2)), the $e_{f,min}$ value that gives highest linearity between $\ln\ln(1-F)^{-1}$ $(= \ln(F)$ in the reduced form) and $\ln(e_f - e_{f,min})$ in eq. (4) is estimated uniquely regardless the range of F concerned. Once $e_{f,min}$ value is obtained, the slope of the $\ln\ln(1-F)^{-1}$ $(= \ln(F)) - \ln(e_f - e_{f,min})$ relation is common for any F and therefore for any n. Accordingly, the m value is determined also uniquely for any F and n. Only the e_0 value is dependent on n. In this way, though the actual number of strut was unknown, the obtained $e_{f,min}$ and m values were reliable.

The following important indications could be read from the present statistical analysis.

(1) Within the accuracy of the electric resistance measured in this work (Fig. 4(a) and (b)), the transition strain from stage II to III could not be identified. The transition strain could be estimated first by the statistical analysis which elucidated the value of $e_{f,min}$ $(= 1.7$ and 0.86% for nickel and copper foams, respectively), corresponding to the transition strain from stage II to III.

(2) Though the e_0 value was dependent on n, it was commonly high for any n (0.24, 0.35 and 0.54 for $n = 4648$, 13944 and 46480, respectively). The average of e_f values, $e_{f,ave}$, is given by $e_{f,ave} = e_0\Gamma(1 + 1/m) + e_{f,min}$. Taking the nickel foam as an example, $e_{f,ave}$ is calculated to be 23, 33 and 50% for $n = 4648$, 13944 and 46480, respectively. In actual foam, n is larger at least than 4648. It is deduced that $e_{f,ave}$ is, at least, higher than 23%. This result indicates that the geometry-affected failure strain of the struts in the foam is very high in comparison with the strain of around 5% (Fig. 4(b)) at ultimate stress of the foam. This means that the struts with lower e_f values (the struts with originally low failure strain and the struts whose longitudinal direction is not so much inclined to the tensile axis) are failed dominantly at low applied strains ($e < 5\%$). The preceding failures of struts act to raise the stress state of the neighboring struts and act as the seeds to cause failures of the struts successively beyond $e = 5\%$. Such a situation takes place at the strain far lower than the average failure strain.

4. Conclusions

Tensile deformation and failure behavior of open cell nickel and copper foams at room temperature was studied experimentally and analytically. The main results are summarized as follows.

(1) The deformation and failure progressed through the following four stages: stage I characterized by elastic deformation up to around 0.01% strain for both nickel and copper foams; stage II by plastic deformation without failure of struts (around 0.01%∼1.7% (nickel foam), around 0.01%∼0.86% (copper foam)); stage III by co-occurrence of plastic deformation and cumulative failure of struts (around 1.7%∼5.2% (nickel foam), around 0.86%∼6.2% (copper foam)); and stage IV by successive failure of struts nearly in a limited cross-section and large increase in electrical resistance with applied strain (5.2%∼ (nickel foam), 6.2%∼ (copper foam)).

(2) The distribution of failure strain of struts in the cumulative failure region was described by the Weibull distribution, from which the strain at transition from stage II to III could be estimated. Also the result of the statistical analysis suggested that the average failure strain of the struts in the foam is much higher than the strain at ultimate stress of the foam.

REFERENCES

1) J. Banhart: Prog. Mater. Sci. **46** (2001) 559–632.
2) L. P. Lefevre, J. Banhart and D. C. Dunand: Adv. Eng. Mater. **10** (2008) 775–787.
3) H. Nakajima: Prog. Mater. Sci. **52** (2007) 1091–1173.
4) D. Leitlmeirr, H. P. Degischer and H. J. Flankl: Adv. Eng. Mater. **4** (2002) 735–740.
5) J. Banhart: J. Mater. **52** (2000) 22–27.
6) H. Nakajima, M. Tane, S. Hyun and S. Suzuki: Materia Japan **47** (2008) 196–202.
7) M. Tane and H. Nakajima: Mater. Trans. **47** (2006) 2183–2187.
8) F. Baumgärtner, I. Duarte and J. Banhart: J. Adv. Eng. Mater. **2** (2000) 168–174.
9) M. Kobashi and N. Kanetake: Materia Japan **47** (2008) 178–181.
10) N. Kanetake, M. Kobashi and S. Tsuda: MetFoam 2007—Proc. 5th Int. Conf. on Porous Metals and Metallic Foams, (Destech Publications, Toronto, 2008) pp. 63–66.
11) M. Wada: Chem. Chem. Industry **54** (2001) 811–813.
12) H. N. D. Wadley: Adv. Eng. Mater. **4** (2002) 726–733.
13) H. Nakajima and T. Ide: Metall. Mater. Trans. A **39** (2008) 390–394.
14) M. Kobashi, K. Kuze and N. Kanetake: Adv. Eng. Mater. **9** (2006) 836–840.
15) N. Kanetake and M. Kobashi: J. High Temp. Soc. **34** (2008) 45–50.
16) Online Materials Information Resource—MatWeb. http://www.matweb.com/search/DataSheet for annealed copper.
17) H. Toda and M. Kobayashi: Materia Japan **47** (2008) 191–195.
18) M. Kobayashi, H. Toda, K. Minami, T. Mori, K. Uesugi, A. Takeuchi and Y. Suzuki: J. JILM **59** (2009) 30–34.
19) W. Weibull: J. Appl. Mech. **28** (1951) 293–297.